Gallium Selenide

Revealing the Preferred Interlayer Orientations and Stackings of Two-Dimensional Bilayer Gallium Selenide Crystals**

*Xufan Li, Leonardo Basile, Mina Yoon, Cheng Ma, Alexander A. Puretzky, Jaekwang Lee, Juan C. Idrobo, Miaofang Chi, Christopher M. Rouleau, David B. Geohegan, and Kai Xiao**

Abstract: Characterizing and controlling the interlayer orientations and stacking orders of two-dimensional (2D) bilayer crystals and van der Waals (vdW) heterostructures is crucial to optimize their electrical and optoelectronic properties. The four polymorphs of layered gallium selenide (GaSe) crystals that result from different layer stackings provide an ideal platform to study the stacking configurations in 2D bilayer crystals. Through a controllable vapor-phase deposition method, bilayer GaSe crystals were selectively grown and their two preferred 0° or 60° interlayer rotations were investigated. The commensurate stacking configurations (AA′ and AB stacking) in as-grown bilayer GaSe crystals are clearly observed at the atomic scale, and the Ga-terminated edge structure was identified using scanning transmission electron microscopy. Theoretical analysis reveals that the energies of the interlayer coupling are responsible for the preferred orientations among the bilayer GaSe crystals.

Two-dimensional (2D) crystals have attracted significant attention in recent years owing to their promising potential applications in electronics, optoelectronics, and energy harvesting.[1] Along with monolayer 2D crystals, few-layer 2D crystals are also very important because they can possess extra and distinct degrees of freedom, such as layer pseudospin, making them even richer systems to study complex electronic states.[2] Recently, there has been growing interest

[*] Dr. X. Li, Dr. L. Basile, Dr. M. Yoon, Dr. C. Ma, Dr. A. A. Puretzky,
  Dr. J. Lee, Dr. J. C. Idrobo, Dr. M. Chi, Dr. C. M. Rouleau,
  Dr. D. B. Geohegan, Dr. K. Xiao
  Center for Nanophase Materials Sciences
  Oak Ridge National Laboratory, Oak Ridge, TN 37831 (USA)
  E-mail: xiaok@ornl.gov

  Dr. L. Basile
  Departamento de Física, Escuela Politécnica Nacional
  Quito (Ecuador)

in 2D bilayer crystals in which the two layers are not only conventionally stacked, but rotated relative to one another at arbitrary angles.[3] For example, bilayer graphene displays tunable bandgaps and exotic electronic properties quite different from monolayer graphene that strongly depend on the rotation angle and stacking registry between the layers.[4] Xu et al. observed the coupling of real spin with layer pseudospin in a given valley in bilayer WSe_2,[5] and a tunable valley magnetic moment through the application of gate bias in bilayer MoS_2.[2c] Despite the scientific importance of these results and the great potential for new applications, comprehensive experimental studies are still lacking that characterize the atomic-scale crystal structure of such bilayer 2D semiconductors, including work on interlayer stacking registry and rotation angle, and understanding how these structures result from particular synthesis conditions.

Gallium selenide (GaSe) is a layered semiconductor widely used in optoelectronics, nonlinear optics, and terahertz radiation detection.[6] The layers of bulk GaSe crystals are bonded to each other by vdW forces. However, a unique feature of the crystal structure of bulk GaSe is that it has four different polytypes, designated as β-(2H), ε-(2H), γ-(3R), and δ-(4H) GaSe,[7] that correspond to different layer stacking and result in different electronic and optical properties.[8] The β- and ε-polytypes have 2H stacking sequences, reflected by two bilayer stacking periodicity and hexagonal symmetry in the crystal unit cell.[7] As shown in the Supporting Information, Figure S1, the β-polytype has inversion symmetry between layers with pairs of Ga and Se atoms in one layer in direct vertical alignment with Se and Ga atoms, respectively, in another, so we designate it AA′-type stacking. The ε-polytype lacks an inversion center, which is called AB-type stacking. Therefore, it is ideal to use bilayer GaSe as a model system to study how the 2D bilayer stacking with different crystal inversion symmetries is related to the polytype of layered bulk crystals.

Recently, 2D GaSe crystals have been synthesized through vapor-phase deposition or epitaxy growth.[9] Previously we synthesized large monolayer GaSe crystals through a controllable vapor-phase deposition method.[9a] In this work, large triangle bilayer GaSe crystals with different interlayer rotations were grown using a modified method in which the argon carrier gas flow rate was tuned. The atomic structures of these bilayer crystals with different interlayer rotations were observed, enabling us to directly relate the interlayer rotations to stacking modes and polytypes. A first-principles approach was used to investigate the energetics of the bilayer stacking with rotation angle, and agreed well with the experimental findings. Our work demonstrates valuable

insight into the stacking modes and interlayer orientations of few-layer 2D semiconductors, and therefore provides useful guidance to study the electronic properties and controlled synthesis of few-layer crystals and van der Waals (vdW) heterostructures.

The 2D GaSe crystals were grown on a Si substrate with a 300 nm thermally grown SiO_2 layer using a process similar to that described in our previous work.[9a] In the synthesis, the argon carrier gas flow rate plays an important role in controlling the thickness of the resulting crystals. To get a high and uniform distribution of bilayer crystals, a 60 sccm Ar flow was used (for detailed methods, see the Supporting Information). Note that in the diffusion-limited growth regime the flux of precursors to the substrate is determined by diffusion through the boundary layer formed near the substrate by this fast flow of Ar, with the flux proportional to the square root of this flow rate.[10] This indicates that only very small increases (ca. 10%) in the precursor flux can result in switching the growth mode from monolayer to bilayer, underlining the importance of precise tuning of the carrier gas flow for deterministic growth.

Figure 1 a,b show typical optical micrograph and scanning electron microscopy (SEM) image of the as-synthesized 2D GaSe crystals. The crystals are all equilateral triangles and contain both monolayer and few-layer flakes. Atomic force microscopy (AFM) images show that most of the few-layer crystals are bilayers (Figure 1 g–i). The top layers of some bilayer crystals have the same size and orientation as the bottom layer (type I stacking, ca. 45% of all the bilayers), as shown in Figure 1 c (the flake indicated as 1) and Figure 1 g (Supporting Information, Figure S2), while others show a shape in which the top layer has a much sharper edge compared with the bottom layer. These bilayer crystals show different interlayer orientations, with a distribution of about 45% for 0° stacking (type II stacking) and about 10% for 60° stacking (type III stacking), and in very rare cases, randomly twisted stacking between 0 and 60° among all the bilayers (type IV stacking). A special case of type III stacking is also observed, that is, the top layer triangle is truncated when it grew to the edges of the bottom layer (Figure 1 c, the flake indicated as 2). The distribution of each type of bilayer crystals was calculated from typical low-magnification SEM images (Supporting Information, Figure S2). The results indicate that the top layer of the bilayer crystals prefer to form with the same orientation as the bottom layer. Interestingly, among the as-synthesized bilayer GaSe crystals, despite the size or orientation of the top layers, they generally share the same geometric center with the underlying layers. This may be explained by defect-mediated growth, because as shown in Figure 1 c–f, small GaSe particles were always observed in the center of most of the triangles, and may assist the growth of successive layers. Figure 1 j shows the Raman spectra of various bilayer GaSe crystals and a multi-layer crystal (ca. 20 layers). The intensity of the Raman peaks decreases dramatically as the crystals are thinned to a bilayer. The Raman spectra of the type I, II, and III bilayer crystals are similar to each other, although the A^1_{1g} peaks (out-of-plane mode) shift slightly to about 131 cm^{-1}. Such a red-shift is likely due to the decrease in interlayer interaction.

The crystal structures of the bilayer GaSe were characterized using both electron diffraction and bright-field imaging in TEM and Z-contrast imaging in aberration-corrected scanning transmission electron microscopy (STEM), respectively. The samples for TEM and STEM characterizations were grown directly on amorphous silicon films (5 nm thick) supported by a silicon TEM grid under the
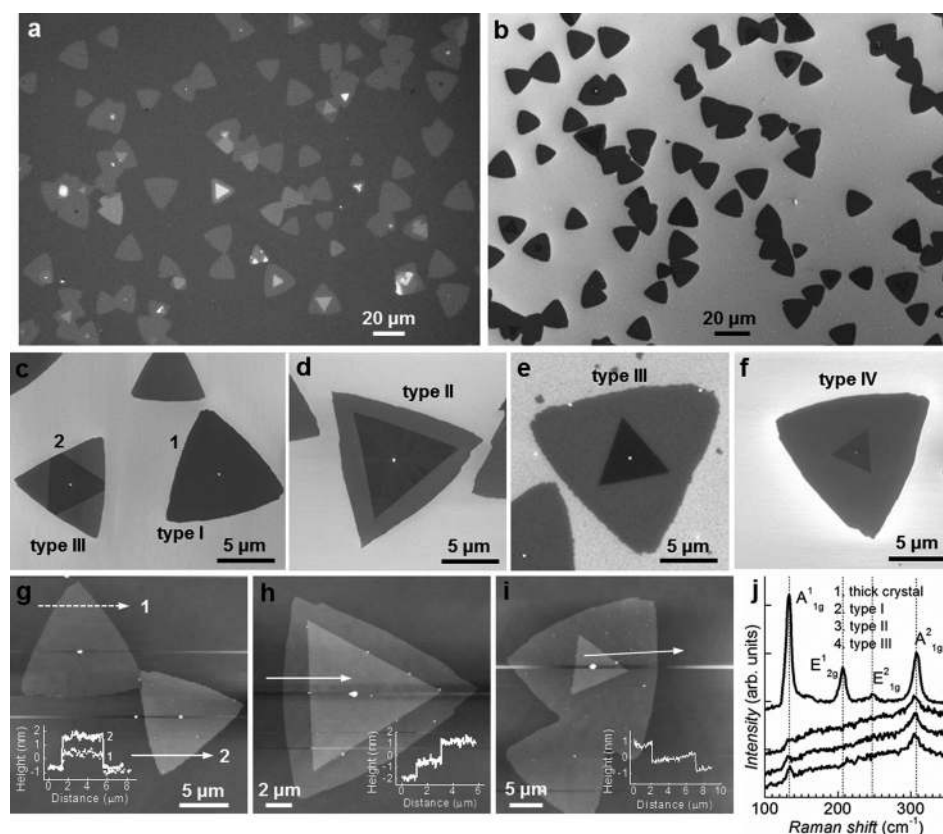

Figure 1. Morphologies of 2D GaSe crystals. a,b) Optical micrograph and SEM image of triangular 2D GaSe containing both monolayer and multi-layer crystals. c–f) Magnified SEM images featuring bilayer crystals with typical stacking orientations. g–i) AFM images of monolayer and bilayer crystals. Insets are line profiles in the direction of the arrows. j) Raman spectra of thick GaSe crystals (curve 1), type I (curve 2), type II (curve 3), and type III (curve 4) bilayer crystals with 532 nm laser excitation. Note that the spectra were offset for clarity.
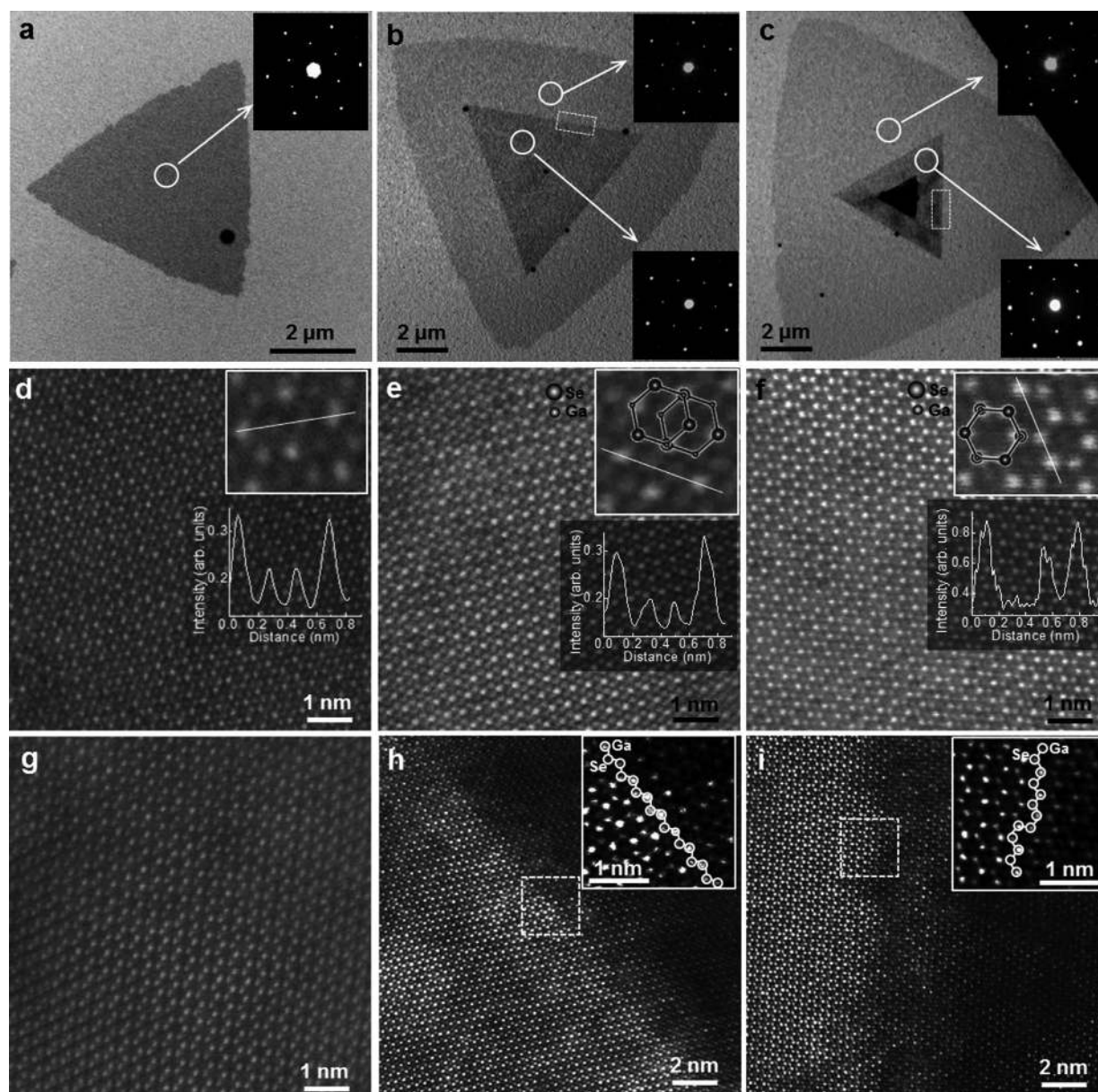
Figure 2. Atomic resolution structures of bilayer GaSe crystals with different stacking modes. a–c) BF-TEM images of bilayer GaSe crystals with type I, II, and III stacking modes, respectively. Insets are SAED patterns from the area indicated by solid circles. d–f) Corresponding Z-contrast STEM images of the bilayer with the three stacking modes, respectively. Insets are magnified images and intensity profiles along the solid lines. g) Z-contrast STEM image of monolayer GaSe. h,i) Z-contrast images showing the edges of the top layer of the type II and III bilayer crystals, as indicated by dashed rectangles in (b) and (c). Insets are magnified images of the area contained by dashed squares. The atoms on the edge are highlighted.

same condition as the growth on SiO_2/Si wafer. Figure 2a–c show the bright-field TEM (BF-TEM) images of individual bilayer GaSe crystals with type I, II, and III stacking, respectively. Note that the flake shown in Figure 2c contains more triangular layers in the center (showing the darkest contrast), and we only studied first two layers with type III stacking in this case. The selected-area electron diffraction (SAED) patterns along the [001] zone axis acquired from both the monolayer and bilayer regions show only one set of six-fold symmetry diffraction spots (insets of Figure 2a–c). For the type II and III stacking, the patterns from the bilayer region are identical to those from the monolayer region but

with a higher intensity. The results indicate that the bilayer GaSe crystals with type I, II, and III stacking are single crystals with hexagonal crystal structures; in other words, the type I, II, and III stacking modes are in a commensurate state.[11]

We used Z-contrast STEM imaging to directly image the stacking with atomic resolution. The type I and II bilayer crystals exhibit close-packed atomic structures, with both brighter (with higher intensity) and darker (with lower intensity) positions (Figure 2d,e), corresponding to atoms in AB stacking as illustrated in the Supporting Information, Figure S1b. The brighter positions, corresponding to atomic

columns, with a hexagonal symmetry and a spacing of ≈ 0.38 nm, in accordance with the lattice parameters of the *ab* plane (0.375 nm), correspond to the sites where two Ga (Se) atoms in one layer are stacked on the top of two Se (Ga) atoms in another, where the coherent scattering makes the intensity higher than the sites with only Ga or Se atoms from one individual layer. The type III crystal shows all atoms in a hexagonal lattice, as is characteristic of AA′-stacked bilayer domains (Figure 2 f). Such a hexagonal ring structure is similar to that of a monolayer GaSe crystal (Figure 2 g). In AA′-stacked bilayer GaSe, all the Ga (Se) atoms in one layer are directly above Se (Ga) in the other, so each atom is visible, and all have similar brightness. The distance between two in-plane adjacent atoms is about 0.32 nm, and very close to $(\sqrt{3}/2)a$. Quantitative simulations of the Z-contrast annular dark-filed (ADF) images and profiles are shown in the Supporting Information, Figure S3, and closely match the experimental ADF profiles in Figure 2. The STEM imaging as well as quantitative simulation of the Z-contrast profiles clearly demonstrate that the type I and II bilayer GaSe crystals with AB stacking belong to the ε-polytype, while the type III with AA′ stacking belong to the β-polytype. In the type III bilayer GaSe, each cation has a remote anion neighbor in the adjacent layer and vice-versa. In the type I and II bilayer GaSe, on the other hand, half the atoms have no opposite neighbor. The polar bonding across the layers will thus be strongest in the type I and II bilayers. Furthermore, the type III bilayer crystal has an inversion symmetry between the layers whereas the type I and II bilayer crystals lack an inversion center. The difference in crystal symmetry in these bilayer GaSe crystals are interesting for future studies of their stacking-order-dependent valley magnetic and excitonic valley pseudospin behaviors.[5, 12]

Edge structures and states in 2D materials play an important role in magnetic, nonlinear optics, photoluminescence, catalysis, and electron dynamics for the quantum Hall effect and topologic insulators.[13] Therefore, the identification of the atomic structure of edges is an important step toward exploring these properties in 2D crystals. The top layers in our bilayer GaSe crystals have much sharper and straighter edges than the bottom layers (Figure 1 d,e), which makes them suitable for imaging edge structures using atomic resolution STEM. ADF-STEM images (Figure 2 h,i) show large intensity contrast between the monolayer and bilayer region, featuring the edge of the top layer with type II and III stacking, respectively. As shown in Figure 2 g–i, the Se atoms are slightly brighter than Ga atoms owing to the larger mass in monolayer GaSe crystals; however, in bilayer GaSe crystals, the brighter spots correspond to pairs of Ga and Se atoms that are stacked in vertical alignment between top and bottom layers, while the less intense spots correspond to Ga or Se atoms that are not aligned vertically. Therefore, as shown in the enlarged images in the insets, based on the atomic structure of bottom layer in bilayer GaSe, we conclude that the edges generally show Ga-terminated zigzag structures.

Compared with type I, II, and III stacking, type IV stacking is very rare in our GaSe crystals. Figure 3 a and b show a GaSe crystal with a region containing 4 layers in the center. A closer look at this multi-layer region shows that the
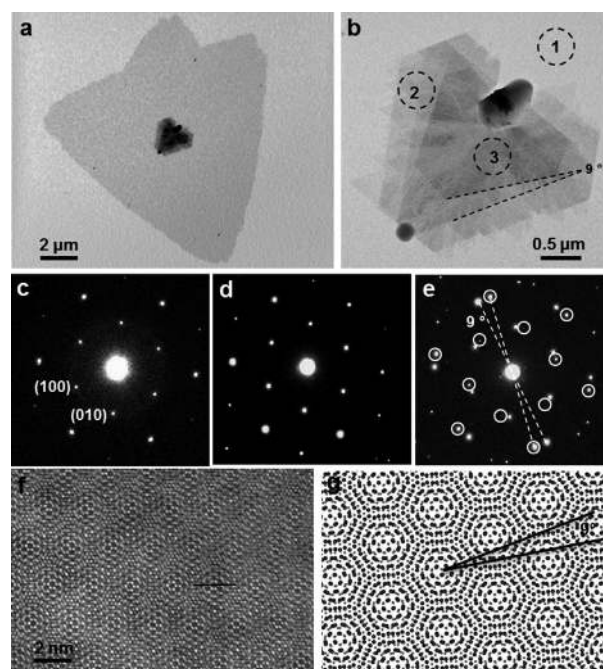

Figure 3. Structures of type IV stacking in a multi-layer GaSe crystal. a) BF-TEM image of a monolayer crystal containing multi-layers in the center. b) Magnified BF-TEM image showing the multi-layer region. c–e) SAED patterns of the monolayer region indicated by circle 1 and the multi-layer regions indicated by circles 2 and 3 in (b), respectively. f) Z-contrast STEM image of the region indicated by the blue circle in (b). The solid line indicates the periodicity length of moiré pattern (g). Atomic model of two monolayer GaSe rotating by 9° with respect to each other.

edges of the two top layers are aligned at 9°. The SAED patterns from the monolayer region and the region containing the first three layers are identical to each other, showing only one set of six-fold symmetry diffraction spots (Figure 3 c and d). However, in the SAED pattern from the region with four layers, along with the spots from the first three layers, another set of hexagonally arranged diffraction spots rotated by about 9° is observed (Figure 3 e). The result indicates that the top layer has an interlayer misorientation of about 9° with respect to the underlying layers, corresponding to the edge alignment shown in Figure 3 b. Such a 9° interlayer misorientation is also reflected by the moiré pattern, which has a periodicity of about 2.3 nm, shown in the Z-contrast image of the 4-layer region (Figure 3 f). For visualization, the atomic model of the two single atomic GaSe layers with a 9° misorientation is illustrated in Figure 3 g. In contrast to type I, II, and III stackings, type IV stacking in this crystal is in an incommensurate state.[14] Previous theoretical and experimental work have already revealed that for the case of twisted bilayer graphene, van Hove singularities, superlattice Dirac points, Hofstadter's butterfly, and the fractional quantum Hall effect manifest on these kind of topological structures with moiré patterns.[15] Therefore, the twisted bilayer GaSe crystal, as a pseudoheterostructure, exhibiting a moiré pattern may be potentially used in solar cells or light emitters with easily tunable bandgap.
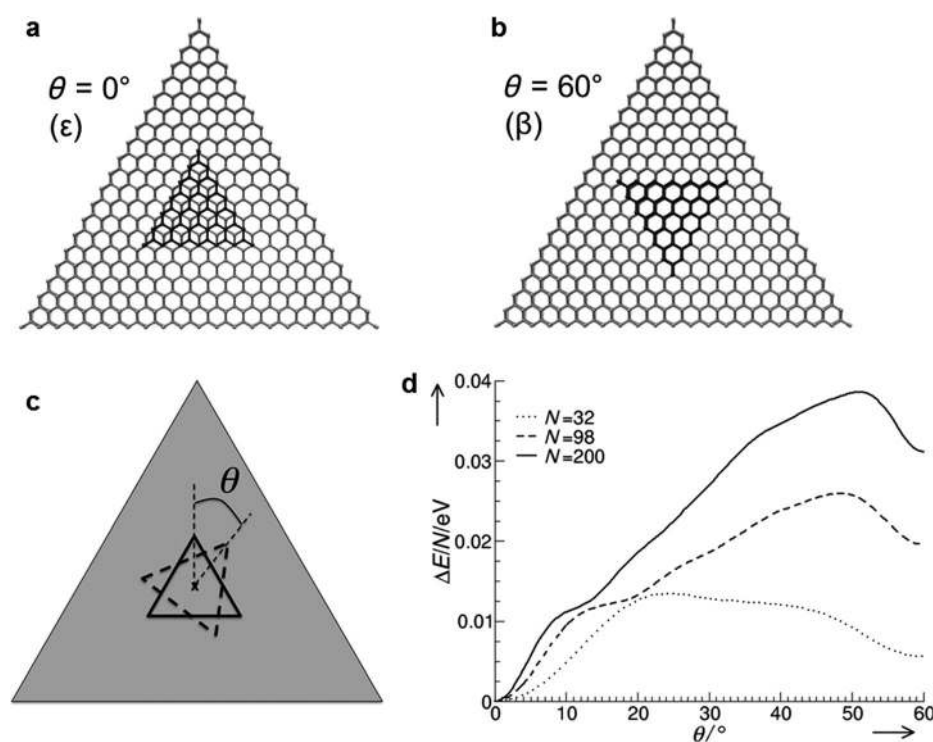
Figure 4. Theoretical modeling of bilayer GaSe crystals. a,b) Illustration of bilayer GaSe with ε-polytype (AB) stacking ($\theta = 0°$) and β-polytype (AA′) stacking ($\theta = 60°$). c) View of the rotation of the top layer with respect to the bottom layer. d) Energy barriers for rotating the top layer with respect to the bottom layer, where rotation angle $\theta = 0°$ corresponds to the ε phase and 60° to the β phase. N denotes the total number of atoms in each layer and the bottom layer consists of 882 Ga and Se atoms.

Theoretical calculations were performed to understand the origin of the interlayer rotations in the GaSe bilayers almost exclusively either 0° or 60°, and Figure 4a and b show two example bilayer structures, where in both cases the top layer is pinned at the center of the bottom layer and a rotation angle (θ) is defined with respect to the bottom layer as shown in Figure 4c. We focus on the configurations of type II ($\theta = 0°$) of the ε-polytype, energetically the most stable bulk phase, which can be converted to the β-polytype (type III) upon a $\theta = 60°$ rotation. We investigated the energetics of different interlayer stacking configurations from type II (AB) to type III (AA′), where the top layer consists of triangular GaSe flakes of different edge lengths of circa 1.12 nm ($N = 32$ atoms), 2.25 nm ($N = 98$ atoms), 3.37 nm ($N = 200$ atoms), and the bottom layer is 7.49 nm long in each side ($N = 882$ atoms). Figure 4d shows the energy per atom of the top layer with respect to the energy minimum configuration of type II. Our calculation shows that the type II (AB) stacking configuration is energetically the most stable for the nano-island configurations, which supports the experimental observation that type II (AB) is the most commonly found stacking mode. The results are also in agreement with previous reports that the main polytype in bulk single crystal of GaSe is the ε-polytype. Our calculations also show that the energetic pathways between the two stable configurations, type II (AB) and type III (AA′), are strongly size-dependent. The rotational energy barriers are higher as the system size increases (Figure 4d). It should be noted that the shape of the

energy profiles is very dependent on the atomic registry between the two layers at each rotation angle. A couple of flat regions in the transition region ($0° < \theta < 60°$) indicate the possibility of capturing a top layer configuration that is rotated at an arbitrary angle. However, the calculations do not reveal a pronounced stable intermediate position, thus the chance to stabilize such a structure is low. This is consistent with experimental observations that interlayer rotations of arbitrary angle (for example, the 9° angle shown in Figure 3g) between 0 and 60° are very rare, and much less common than type I, II (AB), or type III (AA′) stacking.

In summary, triangle-on-triangle bilayer 2D GaSe crystals were synthesized and found to occur with two energetically favored interlayer orientations. Direct atomic-scale characterization of the interlayer stacking orientation was performed using STEM from 2D bilayer crystals grown directly on TEM grids. Theoretical calculations of the interlayer energetics support the experimental observations that GaSe bilayers grow predominantly in the most energetically stable symmetric configuration by AB stacking, corresponding to the bulk GaSe ε-polytype, but also less frequently with a metastable $\theta = 60°$ rotation corresponding to the bulk GaSe β-polytype. The synergistic combination of synthesis, atomic-scale characterization, and theory employed here for GaSe bilayers is an approach that provides the basis to understand how correlated electronic and optical properties emerge in other few-layer 2D crystals and vdW heterostructures.

[1] a) M. Chhowalla, H. S. Shin, G. Eda, L.-J. Li, K. P. Loh, H. Zhang, *Nat. Chem.* **2013**, *5*, 263; b) V. Nicolosi, M. Chhowalla, M. G. Kanatzidis, M. S. Strano, J. N. Coleman, *Science* **2013**, *340*, 1226419.
[2] a) K. F. Mak, K. L. McGill, J. Park, P. L. McEuen, *Science* **2014**, *344*, 1489; b) Y. B. Zhang, T.-T. Tang, C. Girit, Z. Hao, M. C. Martin, A. Zettl, M. F. Crommie, Y. R. Shen, F. Wang, *Nature* **2009**, *459*, 820; c) S. F. Wu, J. S. Ross, G.-B. Liu, G. Aivazian, A. Jones, Z. Y. Fei, W. G. Zhu, D. Xiao, W. Yao, D. Cobden, X. D. Xu, *Nat. Phys.* **2013**, *9*, 149.

[3] a) A. Luican, G. H. Li, A. Reina, J. Kong, R. R. Nair, K. S. Novoselov, A. K. Geim, E. Y. Andrei, *Phys. Rev. Lett.* **2011**, *106*, 126802; b) Z. Yan, Y. Y. Liu, L. Ju, Z. W. Peng, J. Lin, G. Wang, H. Q. Zhou, C. S. Xiang, E. L. G. Samuel, C. Kittrell, V. I. Artyukhov, F. Wang, B. I. Yakobson, J. M. Tour, *Angew. Chem. Int. Ed.* **2014**, *53*, 1565; *Angew. Chem.* **2014**, *126*, 1591.

[4] a) A. H. MacDonald, R. Bistritzer, *Nature* **2011**, *474*, 453; b) S. Shallcross, S. Sharma, E. Kandelaki, O. A. Pankratov, *Phys. Rev. B* **2010**, *81*, 165105.

[5] A. M. Jones, H. J. Yu, J. S. Ross, P. Klement, N. J. Ghimire, J. Q. Yan, D. G. Mandrus, W. Yao, X. D. Xu, *Nat. Phys.* **2014**, *10*, 130.

[6] a) L. Leontie, I. Evtodiev, V. Nedeff, M. Stamate, M. Caraman, *Appl. Phys. Lett.* **2009**, *94*, 071903; b) W. Shi, Y. J. Ding, N. Fernelius, K. Vodopyanov, *Opt. Lett.* **2002**, *27*, 1454; c) K. R. Allakhverdiev, M. Ö. Yetis, T. K. Baykara, E. Y. Salaev, *Laser Phys.* **2009**, *19*, 1092.

[7] A. Kuhn, A. Chevy, R. Chevalier, *Phys. Status Solidi A* **1975**, *31*, 469.

[8] L. Plucinski, R. L. Johnson, B. J. Kowalski, K. Kopalko, B. A. Orlowski, Z. D. Kovalyuk, G. V. Lashkarev, *Phys. Rev. B* **2003**, *68*, 125304.

[9] a) X. F. Li, M.-W. Lin, A. A. Puretzky, J. C. Idrobo, C. Ma, M. F. Chi, M. Yoon, C. M. Rouleau, I. I. Kravchenko, D. B. Geohegan, K. Xiao, *Sci. Rep.* **2014**, *4*, 5497; b) S. D. Lei, L. H. Ge, Z. Liu, S. Najmaei, G. Shi, G. You, J. Lou, R. Vajtai, P. M. Ajayan, *Nano Lett.* **2013**, *13*, 2777; c) M. Mahjouri-Samani, R. Gresback, M. K. Tian, K. Wang, A. A. Puretzky, C. M. Rouleau, G. Eres, I. N. Ivanov, K. Xiao, M. A. McGuire, G. Duscher, D. B. Geohegan, *Adv. Funct. Mater.* **2014**, *24*, 6356; d) Y. B. Zhou, Y. F. Nie, Y. J. Liu, K. Yan, J. H. Hong, C. H. Jin, Y. Zhou, J. B. Yin, Z. F. Liu, H. L. Peng, *ACS Nano* **2014**, *8*, 1485.

[10] C. Li, L. Huang, G. P. Snigdha, Y. F. Yu, L. Y. Cao, *ACS Nano* **2012**, *6*, 8868.

[11] a) E. J. Mele, *Phys. Rev. B* **2010**, *81*, 161405; b) C. R. Woods, L. Britnell, A. Eckmann, R. S. Ma, J. C. Lu, H. M. Guo, X. Lin, G. L. Yu, Y. Cao, R. V. Gorbachev, A. V. Kretinin, J. Park, L. A. Ponomarenko, M. I. Katsnelson, Y. N. Gornostyrev, K. Watanabe, T. Taniguchi, C. Casiraghi, H.-J. Gao, A. K. Geim, K. S. Novoselov, *Nat. Phys.* **2014**, *10*, 451.

[12] a) R. Suzuki, M. Sakano, Y. J. Zhang, R. Akashi, D. Morikawa, A. Harasawa, K. Yaji, K. Kuroda, K. Miyamoto, T. Okuda, K. Ishizaka, R. Arita, Y. Iwasa, *Nat. Nanotechnol.* **2014**, *9*, 611; b) B. Zhu, H. L. Zeng, J. F. Dai, Z. R. Gong, X. D. Cui, *Proc. Natl. Acad. Sci. USA* **2014**, *111*, 11606.

[13] a) K. Kusakabe, M. Maruyama, *Phys. Rev. B* **2003**, *67*, 092406; b) X. B. Yin, Z. L. Ye, D. A. Chenet, Y. Ye, K. O'Brien, J. C. Hone, X. Zhang, *Science* **2014**, *344*, 488; c) H. R. Gutiérrez, N. Perea-López, A. L. Elías, A. Berkdemir, B. Wang, R. Lv, F. López-Urías, V. H. Crespi, H. Terrones, M. Terrones, *Nano Lett.* **2013**, *13*, 3447; d) H. I. Karunadasa, E. Montalvo, Y. J. Sun, M. Majda, J. R. Long, C. J. Chang, *Science* **2012**, *335*, 698.

[14] M. Yankowitz, J. M. Xue, D. Cormode, J. D. Sanchez-Yamagishi, K. Watanabe, T. Taniguchi, P. Jarillo-Herrero, P. Jacquod, B. J. LeRoy, *Nat. Phys.* **2012**, *8*, 382.

[15] a) C. R. Dean, L. Wang, P. Maher, C. Forsythe, F. Ghahari, Y. Gao, J. Katoch, M. Ishigami, P. Moon, M. Koshino, T. Taniguchi, K. Watanabe, K. L. Shepard, J. Hone, P. Kim, *Nature* **2013**, *497*, 598; b) L. A. Ponomarenko, R. V. Gorbachev, G. L. Yu, D. C. Elias, R. Jalil, A. A. Patel, A. Mishchenko, A. S. Mayorov, C. R. Woods, J. R. Wallbank, M. Mucha-Kruczynski, B. A. Piot, M. Potemski, I. V. Grigorieva, K. S. Novoselov, F. Guinea, V. I. Fal'ko, A. K. Geim, *Nature* **2013**, *497*, 594.